# Snapshot of sequential SNARE assembling states between membranes shows that N-terminal transient assembly initializes fusion

Yong Jian Wang, Feng Li, Nicolas Rodriguez, Xavier Lafosse, Christine Gourier, Eric Perez, Frederic Pincet

HAL Id: hal-01297850

https://hal.sorbonne-universite.fr/hal-01297850

Submitted on 5 Apr 2016

Classification:

Major: Physical Sciences

Minor: Biophysics

## Title: Snapshot of sequential SNARE assembling states between membranes shows that N-terminal transient assembly initializes fusion

**Authors:** Yong Jian Wang[1], Feng Li[2], Nicolas Rodriguez[3], Xavier Lafosse[4], Christine Gourier[1], Eric Perez[1], Frederic Pincet[1+]


**Author affiliations:**

[1]Laboratoire de Physique Statistique, École Normale Superieure - PSL Research University, CNRS UMR8550, Sorbonne Universités - UPMC Univ Paris 06, Université Paris Diderot, 24 rue Lhomond, 75005 Paris, France.

[2]Department of Cell Biology, School of Medicine, Nanobiology Institute, Yale University, West Haven, Connecticut 06516, United States.

[3] Laboratoire des Biomolécules, Sorbonne Universités - UPMC Univ Paris 06, École Normale Supérieure - PSL Research University, Département de Chimie, CNRS UMR 7203, 4 Place Jussieu, 75005 Paris, France.

[4] Laboratoire de Photonique et de Nanostructures, Centre National de la Recherche Scientifique UPR20, Route de Nozay, 91460 Marcoussis, France.

[+] Correspondence to: pincet@lps.ens.fr

**Keywords**: SNAREpin | Transient assembly intermediate | Surface Forces Apparatus | Förster Resonance Energy Transfer | Energy

**Abstract**: Many prominent biological processes are driven by protein assembling between membranes. Understanding the mechanisms then entails determining the assembling pathway of the involved proteins. Because the intermediates are by nature transient and located in the intermembrane space, this is generally a very difficult not to say intractable problem. Here, by designing a setup with sphere/plane geometry, we have been able to freeze one transient state in which the N-terminal domains of SNARE (soluble *N*-ethylmaleimide–sensitive factor attachment protein receptor) proteins are assembled. A single camera frame is sufficient to obtain the complete probability of this state with the transmembrane distance. We show that it forms when membranes are 20 nm apart and stabilizes at 8 nm. This setup that fixes the intermembrane distance, and thereby the transient states, while optically probing the level of molecular assembly by Förster Resonance Energy Transfer (FRET) can be used to characterize any other transient transmembrane complexes.

**Significance Statement**: Membrane fusion is the key step in cellular traffic, which is induced by the assembly of membrane protein, namely soluble *N*-ethylmaleimide–sensitive factor attachment protein receptor (SNARE). How the protein assembly induces membrane fusion remains unknown. Answering this question requires the knowledge of the assembly intermediates which cannot be accessed by conventional methods. We developed an instrument to not only freeze a continuous series of intermediates of SNARE assembly but also monitor the formation of these domains. Here, we demonstrate that the N-terminal assembly is the initializing step prior to fusion.

\body
## Introduction
In biology, many critical protein-protein interactions occur between membrane surfaces. These include cell-to-cell adhesion (1) to form tissues (*e.g.* cadherins (2, 3)), infection of cells by enveloped viruses (4, 5) (*e.g.* viral envelope fusion proteins), and secretion when a storage vesicle containing hormones or transmitters (6, 7) fuses with the plasma membrane (this fusion is achieved by soluble *N*-ethylmaleimide–sensitive factor attachment protein receptors (SNAREs)(8)). In each of these examples, the biological process is thermodynamically-coupled and energetically-driven by protein folding/assembly. This means that understanding the molecular mechanism requires a complete characterization of the various intermediate transmembrane protein complexes that appear at different intermembrane distances (Fig. 1A). Two challenges render this characterization difficult. First, because of the energy landscape, the intermediates are transient. Second, observing in the nanometer-scale gap between two membranes remains a challenge. Several existing experimental approaches provide partial information. X-ray crystallography gives atomic level images of the proteins after folding (9, 10), providing a framework but not the pathway. With optical tweezers, continuous unfolding of single molecular complexes can be monitored (11, 12) by applying separation forces. The Surface Forces Apparatus (13, 14) (SFA) provides the only possible way to rigidly control intermembrane separation, the main reaction co-ordinate of this class of folding processes, by fixing the separation between two apposed membranes with subnanometer-level precision, and allows direct measurements of forces (required to unfold the protein) (15-17) (Figs. 1 and 2). With the SFA, a continuous series of folding intermediates can be frozen and their energetics (the energy landscape) determined (15) (Fig. 1A). However, none of these techniques provide the

assembling landscape, i.e. a complete view of the various intermediates that naturally occur during protein folding/assembly between membranes.

SNARE protein assembly, that provides the energy for vesicle fusion in intracellular trafficking, is an archetype transmembrane assembly process in which the molecular landscape is strongly correlated with the membrane separation. In the classical case of synaptic fusion, there are two types of SNARE proteins which include the synaptic vesicle SNARE, Synaptobrevin VAMP2 (v-SNARE), and a heterodimer (t-SNARE) made of the presynaptic plasma membrane SNARE proteins, Syntaxin-1 and SNAP-25. v-SNARE and t-SNARE zipper to form a SNAREpin between the membranes. The efficiency of the fusion process is controlled by subtle molecular details that ensure the right timing and appropriate release of energy at each binding stage. The crystal structure of the SNARE complex (9, 10) shows that SNAREs assemble to form a highly stable coiled-coil made of four parallel helix bundles. Zippering of the coiled-coil proceeds in a stepwise manner with a half-zippered SNARE complex being one of the intermediate state (11, 18), but the sub-molecular details of the zippering process between membranes remain unknown. Notably, it is unclear whether the initial intermediate of SNARE assembly requires the binding of their membrane distal N-terminal regions.

In this article, we demonstrate that, using an SFA equipped with a visualizing setup to observe Förster Resonance Energy Transfer (FRET), we are able to access the intermediates of protein assembly between membranes. We exemplify this by the study of the assembly of SNAREpin and show that the first step towards complete SNARE zippering is the N-terminal assembling, and we determine the exact threshold distance, 8 nm, at which this occurs.

## Results
### FRET/SFA
The SFA is a technique that is widely used to measure the force-distance profile between two surfaces that are often functionalized in order to mimic the surface of a colloidal particle or a biological membrane. The distance between the surfaces is determined with sub-nanometer accuracy in a spectrometer through the position of Fringes of Equal Chromatic Order (FECOs) produced from multiple-beam interferometry with back-silvered mica sheets. The force is measured via the deflection of a spring with calibrated spring constant. This powerful technique has so far been used to address a large number of unresolved scientific questions in a wide range of fields, e.g. fundamental physics (19), soft-matter physics (20) or biology (21). It has also been coupled to numerous other techniques such as friction force measurements (22), electrochemical measurements (23), fluorescence (24, 25) or x-ray diffraction (26), etc. When cognate proteins are anchored on the mica surfaces in order to study their assembling, the subnanometer-level resolution distance of the SFA gives access to geometrical parameters and to the energy landscape of the assembling (15, 27). However, because of the flexibility of these molecules, the force-distance profile does not allow to follow the submolecular details that could provide comprehensive information on the intermediate structures: the assembling landscape. To track the formation of molecular complexes, a distance sensitive phenomenon is required. FRET (28) with its nanometric resolution on the distance between two fluorophores, is an appropriate technique to provide such information. FRET occurs between two fluorophores (29), one of which (the donor) emission spectrum overlaps the absorption spectrum of the other (the

acceptor), and there is energy transfer between the two fluorophores when their separation distance is less than the FRET distance, $R_0$, of the order of a few nanometers.

FRET has so far not been incorporated in an SFA. Combining the two techniques into the FRET/SFA is uniquely suited to freeze the absolute distance between two flat membranes, measure the forces and observe the formation of molecular complexes between the surfaces at the nanometer level (almost the amino-acid level for a protein). So when two molecules (proteins) are labeled, one with a donor and the other one with an acceptor, the proximity of the labeled sites (amino-acids) on two molecules (proteins) can be estimated in one molecular (protein) complex and it becomes possible to establish whether molecules (proteins) are assembled at the level of these labeled sites (amino-acids).

The FRET/SFA we have designed involves the basic version of the SFA with some modifications (Fig. 2). To allow simultaneous measurement of forces and observation of the FRET signal, the detection of a FRET signal coming from the samples must be made compatible with the interferometric distance measurements. This requires that the mica of the upper lens has high transmittance at the wavelengths of the donor excitation and the acceptor emission and good reflectance ~90-95% to observe the FECOs in the other wavelengths. This was made possible by designing an adequate 15 layers multidielectric $Ti_3O_5/SiO_2$ coating. The preparation of this special surface is detailed in the Materials and Methods. The resulting reflectivity spectrum is displayed as the black curve in Fig. S1A; the transmission in the SFA setup configuration is displayed in Fig. S1B. Secondly, a band pass filter is placed at the output of the white light source to transmit only the wavelengths used for the FECOs without interfering with the observation of the FRET signal.

Here, we used the Alexa 488 (donor) / Alexa 647 (acceptor) FRET pair . To excite the donor, a 488nm green laser (Coherent, Sapphire 488-200 mW) is sent to the mica surfaces by means of a long pass dichroic mirror that reflects the 488 nm light to the sample and that also transmits the donor and acceptor emission wavelengths. If FRET occurs, the fluorescence of the acceptor is emitted from the surfaces while the fluorescence of the donor is decreased. At the optical exit of the SFA, a dichroic band-pass beam-splitter reflects the fluorescence emission towards the CCD camera and transmits the FECOs towards the spectrometer. A band pass filter is placed at the entrance of the CCD camera (Princeton Instruments, RTE/CCD-782-V/HS) to transmit only the wavelengths related to the acceptor or the donor. The power of the laser beam is carefully tuned to prevent photobleaching while capturing the fluorescent image; in the experiments presented here, it was set at 20 mW. The CCD camera is used to capture the fluorescent image. A scheme of the optical setup is presented in Fig. 2A and the resulting image of the FECOs in the spectrometer is shown in Fig. 2B.

This sensitive system we have developed allows FRET measurements between probes placed at known locations in the proteins folding/assembling between two bilayers that are brought together (and can be withdrawn) with separation rigidly controlled (Figs. 1B), making it possible to read-out the intra-molecular separations within assembling complexes at each inter-membrane distance. The FRET/SFA can, in parallel, measure forces as in a standard SFA, so that when it is desirable the assembling and energy landscapes can be directly compared.

**SNAREpin formation observed with the FRET/SFA**
We have used this experimental setup with SNAREs that are labeled at their N-terminal region, t-SNARE with Alexa 488 and v-SNARE with Alexa 647 (Fig. 1B). Labeling is obtained by binding the dyes to a single cysteine at the N-terminal of each protein (see supporting information for labeling procedure). The necessary mutations of the SNAREs do not affect their ability to fuse membranes (Fig. S2). Our SNAREs also possess a 12xHis tag at their C terminal that enables their incorporation in the apposing bilayers containing 10% lipids with Nickel in their polar heads (see Material and Methods). The final SNARE density in the membrane is about 1 protein per 200 lipids. It has been previously shown that lipid anchoring the SNARE is sufficient to keep their fusion activity (30). When the two SNARE-decorated membranes are brought together and subsequently separated, adhesion is observed (Fig. 3A). This adhesion vanishes in the control experiments in which t-SNARE is blocked to prevent SNAREpin formation. Simultaneous measurement of the FRET signal when the membranes are contacting shows that SNAREpin form in the contact area. The FRET signal disappears in the case of the control experiment. This indicates that the presence of SNARE complexes is responsible for the observed adhesion (Fig. 3B). We have previously shown that the long range repulsion in the energy profiles presented in Fig. 3A is directly correlated with the local SNARE density (15). Briefly, when the surfaces are between 10 and 20 nm during the approach, the SNARE are not bound yet and they behave like polymers. The repulsion is exponentially decaying with the distance and the prefactor (extrapolated repulsion when the surfaces are in contact) is proportional to the density. Dividing the adhesion energy ~0.2 $k_BT/nm^2$ by the density resulting from this fit directly provides the energy per SNAREpin between the membranes which is $29 \pm 4$ $k_BT$. This value is consistent with that previously measured (15). This confirms that SNAREpins form in a specific and normal manner between the membranes and shows that the FRET/SFA is suitable to study the arrangements and interactions of molecular complexes confined between two surfaces.

The FRET images can be further analyzed based on the fact that a continuous series of folding intermediates of SNAREpin are frozen in the SFA. The geometry of the membranes resembles that of a sphere of radius $R$ facing a flat plane (Fig. 1A). Placing the membranes in close proximity (minimum distance $h_0$) is equivalent to observing simultaneously all separation distances, $h$, while moving at a distance $r$ away from the contact location (Fig 1A):
$h \approx r^2/(2R) + h_0$      (1)
Hence, a picture of the FRET signal over the whole area of the membranes directly provides a snapshot of the N-terminal assembly at all distances. The thickness of the cylindric lens (a few mm), imposes that the objective be far from the mica surface. Hence, the FRET signal remains weak. To increase the signal/noise ratio, we spin-averaged each image by successive rotations around the point of closest distance (see Materials and Methods). The main difficulty is to precisely localize this center of rotation. By testing several positions from the raw FRET signal (Fig. S3C), we estimate that our accuracy, $\delta$, is better than 10 pixels, *i.e.* better than 3 μm. The resulting spin-averaged picture is presented in Fig. 4A. The FRET signal profile with $r$ is displayed in Fig. 4B. It does not change when the membranes are kept in contact for 30 minutes (Fig. 4B and Fig. S4A) and it is reproducible in successive approach-separation cycles (Fig. S4B-E). As expected, the FRET profile is maximum in the center ($r$~0). In the case of the control, there is no FRET signal; the intensity is even minimum in the center. Given the high

distance sensitivity of FRET, the intensity normalized by that at the plateau presented in Fig. 4B actually represents the ratio between the fractions of bound N-terminal regions at $r$ and at the FRET plateau, $F_{FRET}$. Using Eq. 1, it is then possible to determine the variation of $F_{FRET}$ with the membrane separation $h$ from the single image obtained in Fig. 4A (Fig. 4C). Note that the error on $h$ varies as $r\delta/R$, *i.e.* close to 20% in the relevant range ($h$ between 3 nm and 30 nm). $F_{FRET}$ ($h$) is maximum for $h < 8$ nm and is close to zero for $h > 20$ nm. Between 8 nm and 20 nm, the fraction of bound SNAREs decreases almost linearly. This variation is analyzed in the discussion below in view of what is already known on SNARE assembly.

Another direct conclusion that can be drawn from these observations is that SNAREpin formation is reversible. This can be probed by imaging the FRET intensity after the membranes have been separated. Indeed, a non-reversible assembling would keep the SNARE proteins bound upon membrane separation, with the FRET signal unchanged. Conversely, if the SNAREpins have been unraveled, the acceptor dye will be too far from the donor dye (typically 200 nm) to emit any FRET fluorescence. To determine whether the FRET signal disappeared, we computed the difference between the images after separation and the image at contact, just as what was done to determine the FRET signal during the approach phase. The FRET intensity profile from the spin-averaged picture of FRET signal during the separation phase is almost completely superimposable with the one obtained during the approach phase (Fig. S4F), which shows that SNAREpins can be disassembled upon separation.

## Discussion

The $F_{FRET}(h)$ variation is intriguing because we previously reported in independent SFA measurements that there is no adhesion between two SNARE-decorated membranes when their separation is larger than 8 nm. This conclusion was based on the sharp adhesion drop in Fig. 4D and Ref. (15). These two results may seem contradictory: how can SNARE complex start assembling without producing any significant adhesion between 8 and 20 nm? A closer look at the data shows that there is indeed a small adhesion above 8 nm (1.3 $k_BT \pm 2$ $k_BT$ per SNAREpin). This value, which is much smaller than the 35 $k_BT$ observed below 8 nm, may be slightly underestimated (at most 2 $k_BT$) because of the polymer repulsion of the unstructured SNAREs. Hence, it corresponds to a weak state with an energy lower than 5 $k_BT$ per SNAREpin. The weakness of the bond between the N-terminals of SNAREs is therefore compatible with the detection of FRET and with the relative lack of adhesion we previously reported.

We also observed that it was necessary to wait for tens of minutes in close contact before maximum adhesion was achieved in the SFA (15). The adhesion increased with a characteristic time of ~20 min (see Fig. 2b in ref (15)). The reason for this long wait was unknown. We suspected it may come from the confinement and density between the relatively flat surfaces. Here, we also waited for at least 30 minutes before separation and took FRET images at various times during this wait (Fig. 4B and Fig. S4A). We observed that the FRET signal is fully established as soon as the surfaces are in contact. This means that the N-terminal domains of the SNAREs assemble immediately but that the complex is not yet zippered with enough energy to generate adhesion. Hence, the fast setting-up of the FRET also proves the existence of low low-energy state in which a small fraction of the N-terminal residues of the SNARE domains are bound. This weak state is the first one that occurs during SNAREpin formation. Previous optical tweezers measurements showed that, upon separation, SNAREpins oscillate between several intermediate states depending on the force applied to disassemble it (11) but would not have

been able to observe this initial state. However, the final state in the SFA is relatively well characterized (11, 15) and corresponds to a half-zippered state (or possibly zippered beyond). This allows us to separate the 2 situations: upon contact and after 30 minutes in contact.

First, upon contact, N-terminal regions of the SNARE immediately bind in the low energy state. Below 8 nm, virtually all SNAREpins are assembled in their N-terminal region. Between 8 and 20 nm, only a fraction of them are bound; this fraction decreases as $h$ increases. Beyond 20 nm, no SNAREpins are assembled.

Second, after 30 minutes, the SNAREpins have transited towards the half-zippered state for $h < 8$ nm. Above 8 nm, and because there is no easily detectable adhesion, the SNAREpins are only in the weak energy state. These results are summarized in Fig. 4E.

The long delay for the transition towards the half zippered state indicates a high activation energy barrier. Assuming a standard density of the transition time, the activation energy can be written $E_a = k_B T ln(v_0 \tau)$ where $v_0$ is the frequency of escape attempt, $\tau$ the characteristic time and $k_B T$ the thermal energy. In water, for this type of molecules, $v_0$ is between $10^{10}$ s$^{-1}$ and $10^8$ s$^{-1}$ and, here, $\tau \sim 1000$s. This leads to $E_a \sim 25 - 30$ $k_B T$.

These results imply that, *in vivo*, synaptic vesicles must be brought as close as 20 nm, and preferably 8 nm, form the presynaptic plasma membrane to start SNAREpin formation. The long transition time, $\tau$, between the N-terminal weakly bound state and the high energy half-zippered state suggests that an active mechanism exists to accelerate the transition process, possibly through the use of regulatory factors.

This observation of the first transient state during SNARE zippering between membranes shows the sensitivity and efficiency of the FRET/SFA to detect and characterize intermediate structures between closely apposed membranes. It opens up the way to monitor other transmembrane transient states that cannot be observed otherwise.

## Materials and Methods

**Chemicals**
The lipids used in this study are, 1,2-Dimyristoyl-*sn*-Glycero-3-Phosphoethanolamine(DMPE) (850745X), 1,2-Dioleoyl-*sn*-Glycero-3-Phosphocholine (DOPC) (850375C), 1,2-Dioleoyl-*sn*-Glycero-3-[Phospho-L-Serine] (Sodium Salt) (DOPS) (840035C), and 1,2-dioleoyl-*sn*-glycero-3-[(N-(5-amino-1-carboxypentyl)iminodiacetic acid)succinyl] (nickel salt) (NTA-Ni) (79404) which are purchased from Avanti Polar Lipid. More details on buffer and other chemicals are provided in the supporting information.

**SNARE Proteins (Fig. S5)**
*Cytosolic v-SNARE with end-of-sequence 12x Histidine (v-SNARE).* v-SNARE for the FRET/SFA study is made of the cytoplasmic domain of mouse VAMP2 (residues 1-96 with a single Cysteine, S28C, and C-terminal 12x His).
*Cytosolic t-SNARE with end-of-sequence 12x Histidine (t-SNARE).* t-SNARE for the FRET/SFA study is made of the cytoplasmic domain of rat Syntaxin1A (residues 1-265 with a single Cysteine, S193C, and C-terminal 12x His) and mouse His6-SNAP25 (residues 1-206, Cysteine-free).

Details on protein constructs, expression and purification are given in the supporting information.

**Reflective coating on Mica**
The lower mica has the backside surface coated with a 67 nm silver layer prepared by a thermal evaporator in a clean room of Class1000.
The backside of the upper mica has a custom coating made of 15 or 13 alternating $Ti_3O_5$ and $SiO_2$ layers starting with $Ti_3O_5$, with a total thickness of 1.1μm. More precisely, the technique used is an IAD Ion assisted deposition i.e E-beam evaporation (Plassys MEB 800) with ion assistance provided by an ion gun (KRI EH 1000 source). The design, synthesis and refinement of the custom coating have been done theoretically with Essential MacLeod software. Targets of reflectivity, R, have to be set. In our case, we wanted low R (~5%) for both 488nm-520nm and above 660 nm spectral regions and high R (~95%) between 570 nm and 630 nm. The optimization is using $SiO_2$ and $Ti_3O_5$ mean refractive indices for the entire considered spectral range.
From given initial thicknesses to the theoretical stack at an arbitrary wavelength of this range, the algorithm finds solutions with different figures of merit. As an example, for 15 layers, we chose one of these solutions for which the thickness of each layer is (starting from the mica surface): 65.69 nm ($Ti_3O_5$) / 129.59 nm ($SiO_2$) / 72.65 nm ($Ti_3O_5$) / 35.48 nm ($SiO_2$) / 29.32 nm ($Ti_3O_5$) / 182.25 nm ($SiO_2$) / 66.43 nm ($Ti_3O_5$) / 89.79 nm ($SiO_2$) / 79.51 nm ($Ti_3O_5$) / 111.51 nm ($SiO_2$) / 25.16 nm ($Ti_3O_5$) / 24.02 nm ($SiO_2$) / 136.10 nm ($Ti_3O_5$) / 67.05 nm ($SiO_2$) / 94.86 nm ($Ti_3O_5$).
The deposition is made with the following protocol. Both $Ti_3O_5$ and $SiO_2$ are deposited with a rate of 0.25nm/s. Starting materials are $Ti_3O_5$ and $SiO_2$ of 1-3 mm pieces put in Molybdenum liners. To avoid stress issues on the mica that would curve it, we set the ion gun discharge voltage at 100V and discharge Current at 1A. The background pressure before adding gases was $1.0\times10^{-7}$mbars, the working pressure was ~$3.0\times10^{-4}$ mbars with flows of 5sccm for Ar and 5 sccm for the ion source and 10 sccm of Ar for the Keeper (plasma bridge). The layer thicknesses were followed in real time using both a quartz microbalance and an ellipsometer (here, we used 60.5° angle of incidence and 580 nm wavelength).
The reflectivity of the coating is provided in Fig. S1.

**SNARE layer reconstitution**
To prepare the sample for the deposition of the lipid bilayer, the backside-coated mica is glued onto the lens of SFA by thermal epoxy with the coated surface contacting the glue. The mutidielectric coated mica is glued onto the upper lens, and the silver coated mica on the lower lens. Then the lenses are transferred into water and held vertically in a home-built Langmuir trough. The DMPE chloroform solution is directly used as purchased for the first lipid leaflet on both mica surfaces. For the second leaflet, a mixture of the chloroform solutions of DOPC, DOPS and NTA-Ni with the lipid molar ratio of 80%, 10% and 10% was used. The mixture has undergone three freeze (by liquid nitrogen) and thaw cycles to homogenize the solution before use. The rest of the procedure is the same as the one we previously published (15). Details are provided in the supporting information

In the control experiment that follows a fluorescently labeled t- and v-SNARE experiment, the lower lens is taken off from the SFA chamber, kept immersed in buffer in a 5mL beaker and further incubated with non-labeled His-tag free v-SNARE (final concentration of 0.2 μM) at 4$^o$C

overnight. It undergoes the same procedure to rinse off un-bound protein and is remounted into the apparatus.

**SFA force measurement**
A homemade SFA similar to the original design (13) is used, except for the modification on the top mount, as shown in Figs. 1B and 2A. It can adapt a large optical window with the SFA lens at the center. This modification increases the angle through which the emission of the acceptor is collected and therefore improves the optical sensitivity for the FRET signal. The upper lens is initially glued on an optically smooth polished glass slide, provided by Optique Fichou, France. This special upper lens is used in the deposition of the lipid bilayer. One band pass filter (from 570nm to 630nm) is added in front of the white light source, which limits the wavelength range of the fringes for the FECOs but does not disturb the force measurement. The on/off switching of the white light does not give any difference on the intensity of the dark image captured by the CCD camera at the same exposure time for the fluorescent imaging, which proves that the filtered white light source does not interfere with the fluorescent signal. The characteristic wavelengths of the mercury lamp are used for the calibration of the spectrometer. The procedure of the force measurement is the same as described before (15). The spring constant of the cantilever is pre-calibrated and its value is 109N/m.

**Fluorescence Detection**
Genesis MX 488-1000 STM laser purchased from Coherent is used to excite Alexa 488. The laser beam is reflected to the sample by a long pass dichroic mirror with a cut off at 500nm, purchased from Edmunds Optics. In between the laser source and the long pass dichroic mirror, an engineered $20^o$ diffuser from Thorlabs is used to enlarge the illuminated area on the sample. The total optical power illuminating the sample is only about 400μW, as measured by a photo detector. A band pass dichroic beam splitter (transparent from 565nm to 655nm) from Chroma Technology Corp is used to reflect the fluorescent light to the CCD camera while letting the 570 - 630nm light pass to the spectrometer. In front of the CCD camera (Princeton Instruments, RTE/CCD-782-V/HS), there is a multi-filters unit with two band pass filters, both from Edmunds Optics: the transparent wavelength ranges are from 515nm to 560nm and from 650nm to 700nm for the emissions of Alexa 488 and Alexa 647 respectively. The setup of the fluorescent detection is displayed in Fig. 2.

When the separation distance between the samples, controlled by monitoring the fringes, is less than 500nm, one 30% neutral filter is added in front of the laser before turning on the laser to adjust the focus of the fluorescent image. The focus is adjusted with the observation of the fluorescent image of t-SNARE. The 30% neutral filter is also present to capture fluorescent images of t-SNARE, but not for fluorescent images of v-SNARE. The longest exposure time for each fluorescence image is 5s to avoid any bleaching effect or saturation of the detector.

**Spin-Averaged Image and Intensity Profile**
To obtain the spin-averaged image, the initial FRET image (Fig. S4) is rotated 119 times by 3 degrees. This process produces 120 images representing the initial image turned by 0°, 3°, 6°, …, 357°. Then these 120 images are averaged. The whole process is done by a macro programed in Image-J. Intensity profiles such as the one presented in Fig. 4B are plots of the intensity values along a straight line across the center of the spin-averaged image. Because the region close to the

spin center does not contain many pixels to perform the average large fluctuations can be observed. In our system, the data $I_{\text{FRET}}(r)$ of $r$ less than 0.7µm (2 pixels from the center) are not representative of a real average. They should be disregarded for the analysis.

**References:**
1.  Berrier AL & Yamada KM (2007) Cell-matrix adhesion. *Journal of cellular physiology* 213(3):565-573.
2.  Cavallaro U & Christofori G (2004) Cell adhesion and signalling by cadherins and Ig-CAMs in cancer. *Nat Rev Cancer* 4(2):118-132.
3.  Thiery JP (2003) Cell adhesion in development: a complex signaling network. *Curr Opin Genet Dev* 13(4):365-371.
4.  White JM, Delos SE, Brecher M, & Schornberg K (2008) Structures and mechanisms of viral membrane fusion proteins: multiple variations on a common theme. *Crit Rev Biochem Mol Biol* 43(3):189-219.
5.  Harrison SC (2008) Viral membrane fusion. *Nature structural & molecular biology* 15(7):690-698.
6.  Martens S & McMahon HT (2008) Mechanisms of membrane fusion: disparate players and common principles. *Nat Rev Mol Cell Biol* 9(7):543-556.
7.  Rizo J & Rosenmund C (2008) Synaptic vesicle fusion. *Nature structural & molecular biology* 15(7):665-674.
8.  Weber T*, et al.* (1998) SNAREpins: minimal machinery for membrane fusion. *Cell* 92(6):759-772.
9.  Poirier MA*, et al.* (1998) The synaptic SNARE complex is a parallel four-stranded helical bundle. *Nature structural biology* 5(9):765-769.
10. Sutton RB, Fasshauer D, Jahn R, & Brunger AT (1998) Crystal structure of a SNARE complex involved in synaptic exocytosis at 2.4 A resolution. *Nature* 395(6700):347-353.
11. Gao Y*, et al.* (2012) Single reconstituted neuronal SNARE complexes zipper in three distinct stages. *Science (New York, N.Y* 337(6100):1340-1343.
12. Zorman S*, et al.* (2014) Common intermediates and kinetics, but different energetics, in the assembly of SNARE proteins. *eLife* 3:e03348.
13. Israelachvili J & Adams G (1978) Measurement of forces between two mica surfaces in aqueous electrolyte solutions in the range 0-100 nm. *J CHEM SOC FARAD T 1* 74:975-1001.
14. Israelachvili J & Marra J (1986) Direct methods for measuring conformational water forces (hydration forces) between membrane and other surfaces. *Methods in enzymology* 127:353-360.
15. Li F*, et al.* (2007) Energetics and dynamics of SNAREpin folding across lipid bilayers. *Nature structural & molecular biology* 14(10):890-896.
16. Prakasam AK, Maruthamuthu V, & Leckband DE (2006) Similarities between heterophilic and homophilic cadherin adhesion. *Proc Natl Acad Sci U S A* 103(42):15434-15439.
17. Li F*, et al.* (2011) Complexin activates and clamps SNAREpins by a common mechanism involving an intermediate energetic state. *Nature structural & molecular biology* 18(8):941-946.
18. Li F*, et al.* (2014) A half-zippered SNARE complex represents a functional intermediate in membrane fusion. *J Am Chem Soc* 136(9):3456-3464.
19. Tabor D & Winterton RH (1968) Surface forces: direct measurement of normal and retarded van der Waals forces. *Nature* 219(5159):1120-1121.
20. Luckham PF & Klein J (1985) Interactions between Smooth Solid-Surfaces in Solutions of Adsorbing and Nonadsorbing Polymers in Good Solvent Conditions. *Macromolecules* 18(4):721-728.
21. Helm CA, Knoll W, Israelachvili JN, & Gf (1991) MEASUREMENT OF LIGAND RECEPTOR INTERACTIONS. *Proceedings of the National Academy of Sciences of the United States of America* 88(18):8169-8173.

22. Israelachvili JN, Chen YL, & Yoshizawa H (1994) Relationship between Adhesion and Friction Forces. *J Adhes Sci Technol* 8(11):1231-1249.
23. Valtiner M, Banquy X, Kristiansen K, Greene GW, & Israelachvili JN (2012) The Electrochemical Surface Forces Apparatus: The Effect of Surface Roughness, Electrostatic Surface Potentials, and Anodic Oxide Growth on Interaction Forces, and Friction between Dissimilar Surfaces in Aqueous Solutions. *Langmuir* 28(36):13080-13093.
24. Wong JSS, Hong LA, Bae SC, & Granick S (2010) Fluorescence Recovery after Photobleaching Measurements of Polymers in a Surface Forces Apparatus. *J Polym Sci Pol Phys* 48(24):2582-2588.
25. Alig ARG, Gourdon D, & Israelachvili J (2007) Properties of confined and sheared rhodamine B films studied by SFA-FECO spectroscopy. *Journal of Physical Chemistry B* 111(1):95-106.
26. Golan Y*, et al.* (2002) The x-ray surface forces apparatus for simultaneous x-ray diffraction and direct normal and lateral force measurements. *Rev Sci Instrum* 73(6):2486-2488.
27. Perez E, Li F, Tareste D, & Pincet F (2008) The Surface Force Apparatus to Reveal the Energetics of Biomolecules Assembly. Application to DNA Bases Pairing and SNARE Fusion Proteins Folding. *Cellular and Molecular Bioengineering* 1(4):240-246.
28. Stryer L & Haugland RP (1967) Energy transfer: a spectroscopic ruler. *Proc Natl Acad Sci U S A* 58(2):719-726.
29. Helms V (2008) *Principles of Computational Cell Biology* (Wiley-Blackwell).
30. McNew JA*, et al.* (2000) Close is not enough: SNARE-dependent membrane fusion requires an active mechanism that transduces force to membrane anchors. *J Cell Biol* 150(1):105-117.
31. Melia TJ, et al. (2002) Regulation of membrane fusion by the membrane-proximal coil of the t-SNARE during zippering of SNAREpins. J Cell Biol 158(5):929-940.
32. Weninger K, Bowen ME, Choi UB, Chu S, & Brunger AT (2008) Accessory proteins stabilize the acceptor complex for synaptobrevin, the 1 : 1 syntaxin/SNAP-25 complex. Structure 16(2):308-320.
33. Xiao WZ, Poirier MA, Bennett MK, & Shin YK (2001) The neuronal t-SNARE complex is a parallel four-helix bundle. Nature structural biology 8(4):308-311.

**FIGURE LEGENDS**

**Fig. 1 Transient transmembrane molecular intermediates - how to visualize them**

 **(A)** Top: Two molecules assemble to form a molecular complex between a spherical surface and a flat surface with a fixed closest separation distance, $h_0$, at the center. This geometry is the same as that in the FRET/SFA. As the surfaces come closer, the level of assembly of the molecules increases. This is represented in the lower panel cross section in which the complex formed by two imaginary molecules A and B exhibits 4 distinct states: disassembled (left), two intermediate states (middle) and fully assembled (right). In the case of the geometry presented here, when the surfaces are covered with molecules A and B respectively, the level of molecular assembly varies with the distance $r$ to the closest approach on the right hand side of the diagram because the separation distance increases gradually with $r$. Hence, at a given $r$, because the local separation distance is fixed, assembling may only proceed until a certain level, and therefore the two molecules are trapped in an intermediate state. Then, a single snapshot is sufficient to observe all the intermediate states at various $r$ and therefore at all separation distances. In the presented situation, when $r$ is larger than $r_1$, molecules A and B are not bound. Between $r_1$ and $r_2$ they are in intermediate state 1, between $r_2$ and $r_3$ intermediate state 2 is reached and below $r_3$, the complex is fully assembled. Considering three regions in molecules A and B, a membrane distal region (blue), an middle region (orange) and a membrane proximal region (green), each state can be fully identified. When none of the regions are bound, the molecules are disassembled. If the blue regions are the only ones bound, the molecular complex is in the transient intermediate state 1. If regions blue and orange are assembled but not the green ones, it is in intermediate state 2. When all regions are bound, the complex is fully assembled. **(B)** SNARE proteins are used to represent molecules A and B. They zipper into a four-helix coiled coil between the membranes. *In vivo*, the progression of the zippering brings the two membranes together and drives them to fuse. The cytosolic domains are His-tagged to be bound to NTA(Ni)-lipids, mimicking the natural transmembrane anchorage. The membranes are deposited on a mica sheet the other side of which is coated with silver (bottom) or a custom made multi-dielectric layer. This setup allows the simultaneous measurement of the intermembrane separation distance by interferometry and the visualization of FRET signal between SNAREs that are labeled with dyes in their N-terminal regions (excitation at 488 nm). The intermembrane distance can be frozen, just as in (A), in which case, all intermembrane distances can be observed along $r$.


**Fig. 2 Diagram of the FRET/SFA setup**
**(A)** The optical pathways for the SFA fringes, fluorescence excitation and fluorescence emission are denoted by orange, blue and red lines respectively. For the SFA, the modified top mount can adapt the optical window with the large diameter. The 30% neutral density filter (ND filter) is presented in the optical pathway only during the time period of either adjusting the focus or imaging the fluorescently labeled t-SNARE. A magnification of the interacting surfaces is shown in detail in Fig. 1B. **(B)** Resulting image and spectrum of the FECOs in the spectrometer by this setup. The range of wavelengths used for force measurements, *i.e.* for observation of the FECOs, is 570 – 630 nm. A single-line home-made camera with 6000 pixels captures the spectrum along the white dashed line. The resulting intensities are presented below. Out of this range of wavelengths, only fluorescence (or FRET) can pass through the upper multi-dielectric layer presented in Fig. 1B.

**Fig. 3**. **Correlation between adhesion and SNARE N-terminal binding**
FRET/SFA can measure interaction energies while the surfaces are approached and subsequently separated. Simultaneously, the FRET signal (*i.e.* the assembly of the molecular complex) can be monitored at any separation distance. **(A)** SNARE induced adhesion between membranes. In black, the energy per SNAREpin is presented during an approach/separation cycle. During the approach (open disks) only positive, unfavorable energy is observed. Upon separation (closed disks), negative, favorable energy is measured, indicating the SNAREs have assembled. The maximum energy, corresponding to the SNARE binding energy, is the maximum one, *i.e.* $e_m \sim$ 30 $k_B$T here. The red disks represent an approach/separation cycle in the control experiment in which Alexa488 labeled t-SNARE is blocked by pre-incubation with non-labeled and His-tag free v-SNARE. No adhesion is observed in the control experiment, showing unambiguously that the adhesion observed in the fluorescently labeled t- and v-SNARE experiments is SNARE assembling induced. **(B)** FRET signal is correlated with the adhesion of the membranes. The measurement of the FRET signal at the closest separation distance during the approach separation cycle is strongly correlated with the presence of adhesion: a positive FRET signal is observed only when there is adhesion, *i.e.* in the fluorescently labeled t- and v-SNARE experiment. Control experiments do not display any FRET signal. The relative intensity of the FRET signal, $I_{FRET}$ is equal to the mean value of the fluorescent intensity before it decays minus that of the control experiment (plateau in Fig. 4B). The FRET intensities and the corresponding adhesion energies in the FRET/SFA and control experiments were measured repeatedly and at different positions on each sample. The mean values are presented in the plot.

**Fig. 4.** **Stable N-terminal assembly is required for initial binding of the SNAREs**
**(A)** Left: spin-averaged picture (see Materials and Methods and Fig. S3) of the FRET signal between two membranes decorated with fluorescently labeled t- and v-SNARE respectively. Right: spin-averaged picture of the FRET signal in the control experiment. The scale bar represents 20μm. The intensities taken along the dashed line through the center to form the intensity profiles are displayed in **(B)**: $I_a$ (black and red lines) represents the intensity of the fluorescently labeled t- and v- SNARE experiment while $I_c$ (blue) is the control. *r* equals 0 at the center. The black line shows the intensity right after the contact, and the red line was obtained after the surfaces were kept in contact for 30 min. The two lines are overlapping, revealing no time-dependence of the FRET signal. The variation in $I_c$ are due to optical interferences. Hence, the actual FRET signal is the difference between $I_a$ and $I_c$. **(C)** Fraction of the N-terminal assembly in the total population of SNARE pairs with the intermembrane separation distance *h* (obtained from *r* through the equation provided in the main text). The N-terminal domains are only 100% assembled when $h < 8$ nm. The error bars are standard deviation obtained by averaging 20 to 40 data points on 4 separate experiments. **(D)** Adhesion of t- and v-SNARE decorated membranes in the SFA with $h_0$, the minimal intermembrane separation reached during the approach/separation cycle, is normalized by the strongest adhesion (same data as in (15)). The membranes were kept at distance $h_0$ for at least 20 min. **(E)** Various SNARE complex states in the SFA, their respective energies and the distribution of these states after 0 and 30 min in contact at $h=8$ nm, 13 nm and 20 nm. Solid bars represent 0 min and open columns represent 30 min.
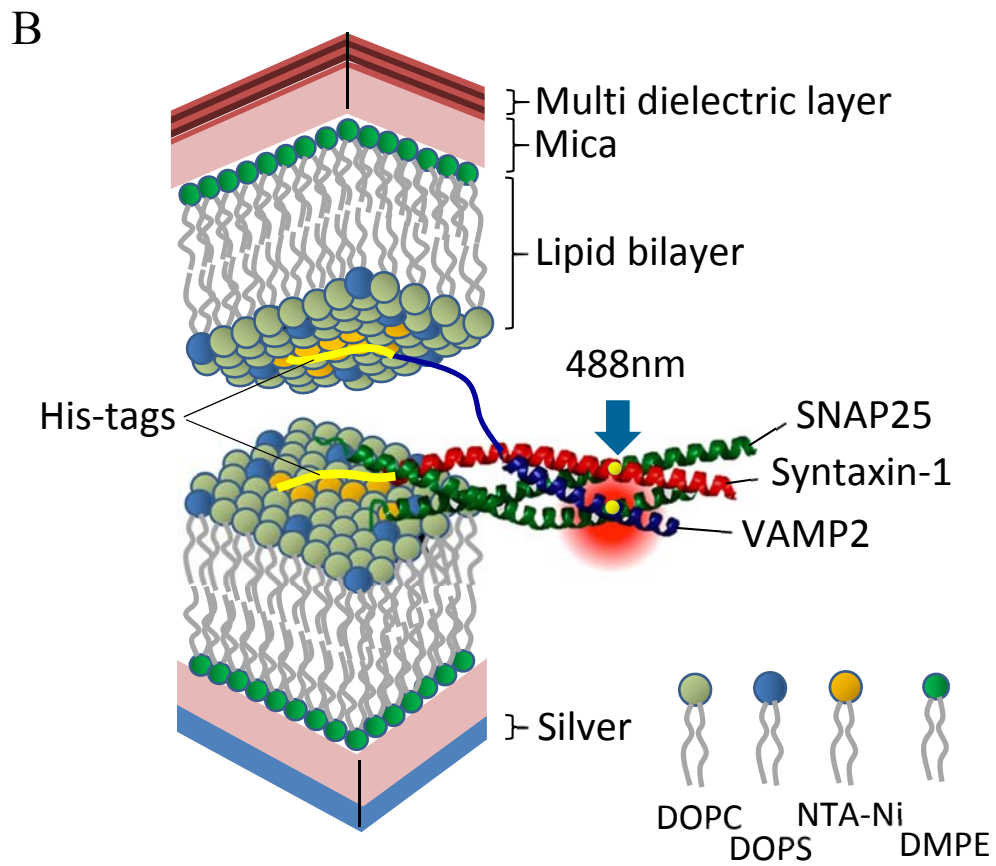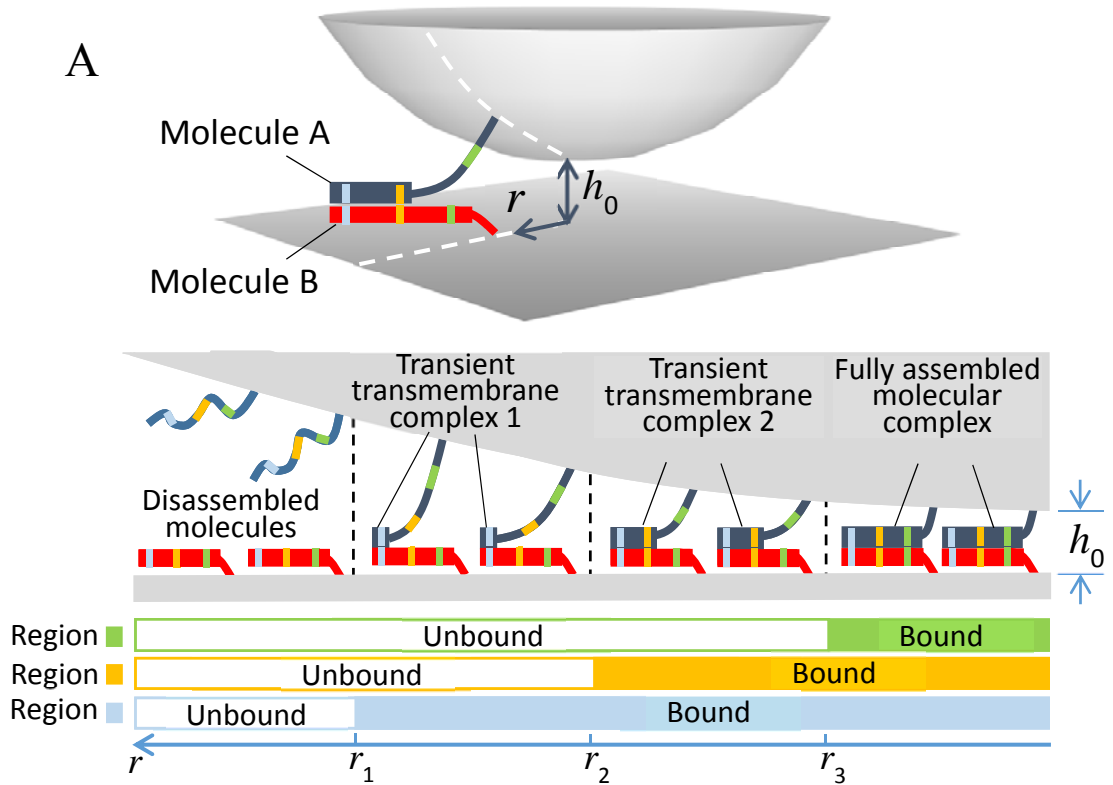
**A**

Molecule A

Molecule B

$r$ $h_0$

Disassembled molecules

Transient transmembrane complex 1

Transient transmembrane complex 2

Fully assembled molecular complex

$h_0$

Region ▢ Unbound / Bound

Region ▢ Unbound / Bound

Region ▢ Unbound / Bound

$r$ $r_1$ $r_2$ $r_3$

**B**

Multi dielectric layer

Mica

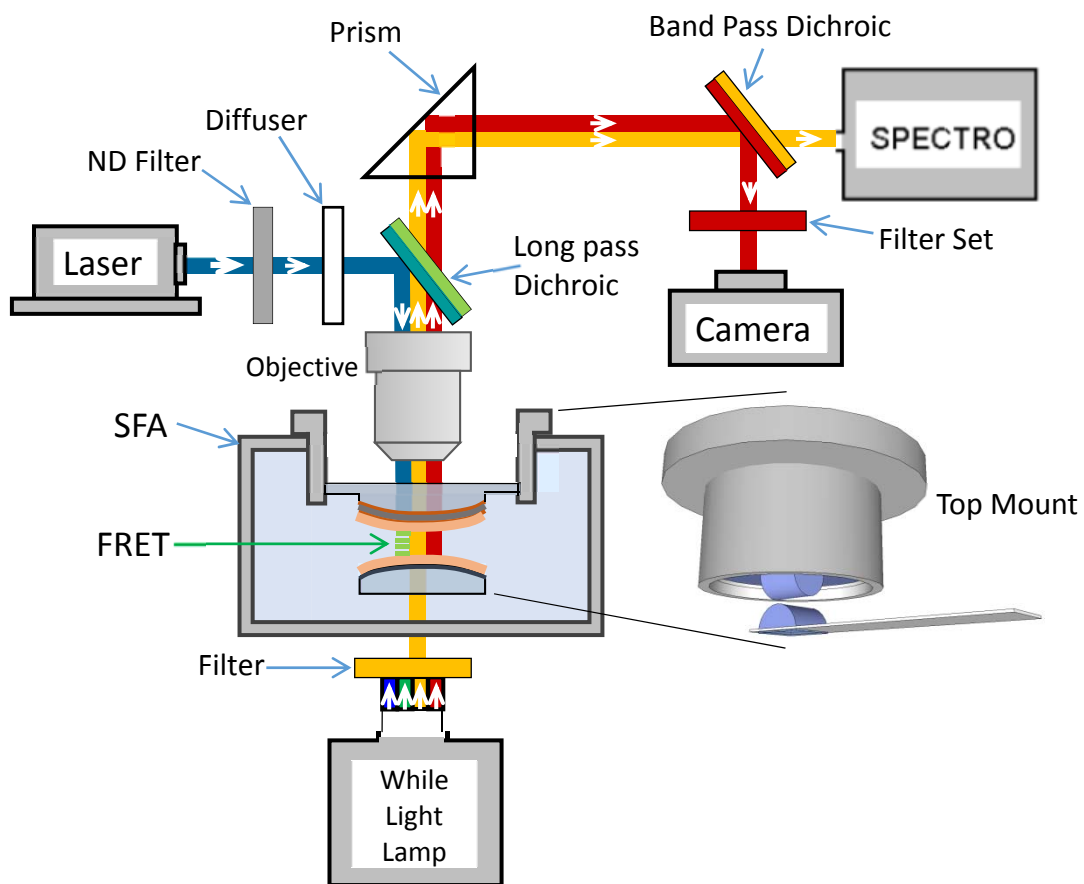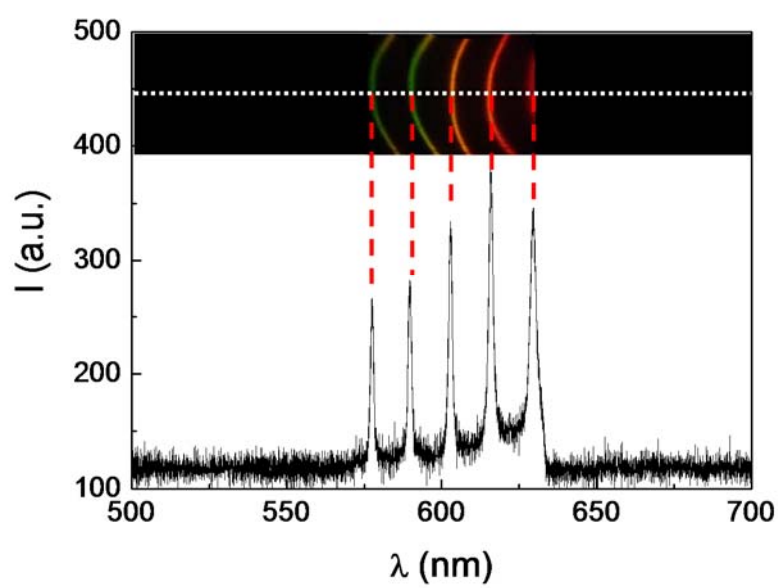Lipid bilayer

His-tags

488nm

SNAP25

Syntaxin-1

VAMP2

Silver

DOPC DOPS NTA-Ni DMPE

Figure 1

A



B



Figure 2

Figure 3

Figure 4



A

FRET    No FRET

B

C

D

Strong
Adhesion

Weak
Adhesion

E

Fraction

*Separated*    *N-terminal assembly*    *~ Half-zipped*

100%

50%

0%

20nm    13nm    8nm          20nm    13nm    8nm          20nm    13nm    8nm
No adhesion (0 k$_B$T)    Weak adhesion (< ~5 k$_B$T)    Strong adhesion (~30 k$_B$T)

■ 0 min
□ 30 min